

A New Type of Axis–Angle Attitude Control Law for Rotational Systems: Synthesis, Analysis, and Experiments

Francisco M. F. R. Gonçalves, Ryan M. Bena, and Néstor O. Pérez-Arcibia

Abstract—Over the past few decades, continuous quaternion-based attitude control has been proven highly effective for driving rotational systems that can be modeled as rigid bodies, such as satellites and drones. However, methods rooted in this approach do not enforce the existence of a unique *closed-loop* (CL) equilibrium attitude-error quaternion (AEQ); and, for rotational errors about the attitude-error Euler axis larger than π rad, their proportional-control effect diminishes as the system state moves away from the stable equilibrium of the CL rotational dynamics. In this paper, we introduce a new type of attitude control law that more effectively leverages the attitude-error Euler axis-angle information to guarantee a unique CL equilibrium AEQ and to provide greater flexibility in the use of proportional-control efforts. Furthermore, using two different control laws as examples—through the construction of a strict Lyapunov function for the CL dynamics—we demonstrate that the resulting unique equilibrium of the CL rotational system can be enforced to be uniformly asymptotically stable. To assess and demonstrate the functionality and performance of the proposed approach, we performed numerical simulations and executed dozens of real-time tumble-recovery maneuvers using a small quadrotor. These simulations and flight tests compellingly demonstrate that the proposed axis-angle-based method achieves superior flight performance—compared with that obtained using a high-performance quaternion-based controller—in terms of stabilization time.

I. INTRODUCTION

The specialized literature has reported extensive research on attitude control methods for rotational systems that can be modeled as rigid bodies, including satellites, drones, and microswimmers [1]–[19]. In this context, we can distinguish three main types of prevalent controllers: quaternion-based [1]–[8], Euler-angle-based [9]–[11], and rotation-matrix-based (geometric) [12]–[14]. By contrast, the published research on attitude control directly based on the Euler axis-angle representation—despite its multiple advantages—is scarce, although the relevant information required to adopt this approach is contained in the rotation matrices and quaternions employed by other methods. For example, in the formulation of quaternion-based attitude control laws, typically, a proportional torque term is defined by simply multiplying the vector part of the instantaneous

The research presented in this paper was supported by the Joint Center for Aerospace Technology Innovation (JCATI) through Award 172, the Washington State University (WSU) Foundation and the Palouse Club through a Cougar Cage Award to N.O. Pérez-Arcibia, and the WSU Voiland College of Engineering and Architecture through a start-up fund to N.O. Pérez-Arcibia.

F.M.F.R. Gonçalves and N.O. Pérez-Arcibia are with the School of Mechanical and Materials Engineering, Washington State University (WSU), Pullman, WA 99164-2920, USA. R.M. Bena is with the Department of Mechanical and Civil Engineering, California Institute of Technology, Pasadena, CA 91125-2100, USA. Corresponding authors' email: francisco.goncalves@wsu.edu (F.M.F.R.G.); n.perezarcibia@wsu.edu (N.O.P.-A.).

attitude-error quaternion (AEQ) by a positive-definite matrix, which therefore includes a $\sin \frac{\Theta_e}{2}$ factor, in which Θ_e is the instantaneous rotation error about the attitude-error Euler axis. It appears that the only rationale behind this design choice is to simplify the mathematical analysis of the *closed-loop* (CL) system dynamics. Additionally, in most reported applications, the proportional term in the quaternion-based law is modified through a switching condition, included to avoid unwinding behavior by forcing the controller to apply the proportional torque effort in the direction of the shortest rotational trajectory required to eliminate the attitude error [4]–[8]. Simple analyses indicate that geometric controllers also apply torque in this direction of shortest rotation, which—as experimentally shown in [1]–[3]—is not necessarily the best choice for every kinematic situation.

In this paper, we present a new type of axis–angle law to control the attitude of rigid-body rotational systems, which guarantees the existence of a unique CL fixed AEQ and does not diminish the proportional-control effort as the system state moves away from the stable CL fixed AEQ—quantified as a rotation about the Euler axis determined by the instantaneous CL AEQ. This research was prompted by phenomena observed during the development and implementation of quaternion-based switching schemes conceived to account for both the direction and magnitude of the flier’s angular velocity—in order to heuristically minimize a figure of merit—when choosing the direction in which the proportional torque control effort is applied [1]–[3]. As a result, these controllers often exert the proportional torque in the direction of the longest rotational trajectory required to eliminate the attitude error—i.e., rotations larger than π rad—which highlights the potential practical utility of this proposed control approach when used in combination with those types of schemes. Furthermore, using two different control laws as examples—through the construction of a strict Lyapunov function for the CL dynamics—we demonstrate that the resulting unique equilibrium of the CL rotational system can be enforced to be uniformly asymptotically stable by satisfying a positive-definite condition. To test and demonstrate the suitability of the proposed approach, we implemented numerical simulations and performed dozens of real-time tumble-recovery maneuvers using a 32-g quadrotor. The obtained simulation and experimental data provide compelling evidence of the high performance characteristic—in terms of stabilization time—of controllers synthesized using attitude laws of the proposed type.

The rest of the paper is organized as follows. Section II provides an overview of the open-loop attitude dynamics of a generic rigid-body rotational system, and describes the synthesis of the quaternion-based controller used as the starting point of the presented research and benchmark. Section III

describes the proposed axis–angle attitude control approach, presents the synthesis of two controllers, and discusses the stability of the fixed points associated with the two resulting CL dynamics. Section IV presents numerical simulations and experimental results—obtained using a small quadrotor—that demonstrate the functionality and high performance—measured in terms of stabilization time—of the introduced methodology. Last, Section V summarizes the results presented in the paper, discusses some conclusions, and states a direction for future research.

Notation-

- 1) Italic lowercase and Greek symbols represent scalars, e.g., p and Θ ; bold lowercase symbols represent vectors, e.g., \mathbf{p} ; bold uppercase symbols represent matrices, e.g., \mathbf{P} ; and, bold crossed lowercase symbols represent quaternions, e.g., \mathbf{p} .
- 2) The sets of integers, nonnegative integers, and positive integers are denoted by \mathbb{Z} , $\mathbb{Z}_{\geq 0}$, and $\mathbb{Z}_{> 0}$, respectively. Similarly, the sets of reals, nonnegative reals, and positive reals are denoted by \mathbb{R} , $\mathbb{R}_{\geq 0}$, and $\mathbb{R}_{> 0}$, respectively.
- 3) The set of unit quaternions is denoted by \mathcal{S}^3 . The special orthogonal group in the three-dimensional space is denoted by $\mathcal{SO}(3)$.
- 4) The symbol \times denotes the cross-product between two vectors. Multiplication between two quaternions is denoted by \otimes .
- 5) The symbols \succ , \prec , \succeq , and \preceq denote definiteness relationships between Hermitian matrices.

II. BACKGROUND

In this section, we briefly review the attitude dynamics of a generic rigid-body rotational system and the basic structure of the quaternion-based controller used as the starting point for the presented research and as a benchmark. As indicated in Fig. 1, $\mathcal{N} = \{n_1, n_2, n_3\}$ and $\mathcal{B} = \{b_1, b_2, b_3\}$ denote the inertial and body-fixed frames of reference used for kinematic and dynamic modeling, respectively. As is customary, \mathcal{N} is fixed to the planet Earth, and the origin of \mathcal{B} coincides with the *center of mass* (CoM) of the modeled rotational system. As discussed in [4], [5], using quaternions and Euler's second law, we can describe the open-loop rotational dynamics of the modeled system as

$$\begin{aligned} \dot{\mathbf{q}} &= \frac{1}{2} \mathbf{q} \otimes \begin{bmatrix} 0 \\ \boldsymbol{\omega} \end{bmatrix}, \\ \dot{\boldsymbol{\omega}} &= \mathbf{J}^{-1} [\boldsymbol{\tau} - \boldsymbol{\omega} \times \mathbf{J} \boldsymbol{\omega}], \end{aligned} \quad (1)$$

where \mathbf{q} is a unit quaternion that represents the orientation of \mathcal{B} relative to \mathcal{N} ; $\boldsymbol{\omega}$ is the angular velocity of \mathcal{B} relative to \mathcal{N} , written in \mathcal{B} coordinates; \mathbf{J} is the inertia matrix of the modeled rotational system, written in \mathcal{B} coordinates; and, $\boldsymbol{\tau}$ is the torque applied to the system and, in closed loop, generated by a control law. As is well known, $\mathbf{q} = [m \ \mathbf{n}^T]^T$, with $m = \cos \frac{\Theta}{2}$ and $\mathbf{n} = \mathbf{u} \sin \frac{\Theta}{2}$, where \mathbf{u} is the Euler rotation axis and Θ is the amount that \mathcal{N} must rotate about \mathbf{u} to be aligned with \mathcal{B} .

For the purposes of controller synthesis, we define the instantaneous AEQ of the modeled rotational system as

$$\mathbf{q}_e = \mathbf{q}^{-1} \otimes \mathbf{q}_d, \quad (2)$$



Fig. 1. Photograph of the quadrotor—a Crazyflie 2.1—used in the flight tests performed to assess and demonstrate the functionality and performance of the proposed attitude control approach. Here, $\mathcal{N} = \{n_1, n_2, n_3\}$ and $\mathcal{B} = \{b_1, b_2, b_3\}$ denote the inertial and body-fixed frames used for kinematic description and dynamic modeling. As customary, \mathcal{N} is fixed to the planet Earth and the origin of \mathcal{B} coincides with the CoM of the controlled rotational system.

where the desired attitude quaternion, \mathbf{q}_d , represents the rotation from the inertial frame, \mathcal{N} , to the desired body-fixed frame, \mathcal{B}_d . Consistently, $\mathbf{q}_e = [m_e \ \mathbf{n}_e^T]^T$ represents the rotation from the current body-fixed frame, \mathcal{B} , to the desired body-fixed frame, \mathcal{B}_d . Namely, $m_e = \cos \frac{\Theta_e}{2}$ and $\mathbf{n}_e = \mathbf{u}_e \sin \frac{\Theta_e}{2}$, where \mathbf{u}_e is the Euler axis about which the controlled rotational system must be rotated an amount $\Theta_e \in [0, 2\pi)$ rad to align \mathcal{B} with \mathcal{B}_d . In agreement with the requirements for controller synthesis imposed by the second line of (1), directly from (2), it follows that \mathbf{u}_e is written in \mathcal{B} coordinates. Also, for real-time implementation, we must compute the desired angular velocity of the controlled rotational system, written in \mathcal{B} coordinates. This computation can be performed in two steps. First, we compute the desired angular velocity of the system in \mathcal{B}_d coordinates as

$$\begin{bmatrix} 0 \\ \dot{\boldsymbol{\omega}}_d \end{bmatrix} = 2\mathbf{q}_d^{-1} \otimes \dot{\mathbf{q}}_d. \quad (3)$$

Then, to obtain the desired angular velocity of the system in \mathcal{B} coordinates, we consecutively apply two transformations, \mathbf{S}_d and \mathbf{S}^T , as

$$\boldsymbol{\omega}_d = \mathbf{S}^T \mathbf{S}_d \dot{\boldsymbol{\omega}}_d, \quad (4)$$

where \mathbf{S}_d transforms vectors from \mathcal{B}_d to \mathcal{N} coordinates, and \mathbf{S}^T transforms vectors from \mathcal{N} to \mathcal{B} coordinates.

Next, as a starting point for the new research presented in this paper, employing the definitions of \mathbf{q}_e and $\boldsymbol{\omega}_d$, we define the control torque input

$$\boldsymbol{\tau}_b = \mathbf{J} [k_\Theta \mathbf{n}_e + k_\omega \boldsymbol{\omega}_e + \dot{\boldsymbol{\omega}}_d] + \boldsymbol{\omega} \times \mathbf{J} \boldsymbol{\omega}, \quad (5)$$

where $k_\Theta, k_\omega \in \mathbb{R}_{> 0}$; $\boldsymbol{\omega}_e = \boldsymbol{\omega}_d - \boldsymbol{\omega}$ is the angular-velocity tracking error; $\mathbf{J} \dot{\boldsymbol{\omega}}_d$ is a feedforward term that cancels the left-hand side of the second equation in (1) and provides faster tracking performance; and, $\boldsymbol{\omega} \times \mathbf{J} \boldsymbol{\omega}$ is a feedback-linearization term that cancels the nonlinearity in the second equation of (1). As shown in [4], the CL attitude dynamics resulting from substituting the *right-hand side* (RHS) of (5) into (1) exhibit two equilibria, specified by the pairs $\{\mathbf{q}_e^*, \boldsymbol{\omega}_e^*\}$ and $\{\mathbf{q}_e^\dagger, \boldsymbol{\omega}_e^*\}$, with $\mathbf{q}_e^* = [+1 \ 0 \ 0 \ 0]^T$, $\mathbf{q}_e^\dagger = [-1 \ 0 \ 0 \ 0]^T$, and $\boldsymbol{\omega}_e^* = [0 \ 0 \ 0]^T$. These two points define the same kinematic situation, but with different stability

properties—one asymptotically stable and the other unstable. As expected from basic nonlinear theory, given that at both fixed points it occurs that $\mathbf{n}_e = \mathbf{0}$, if the system state were to exactly reach the unstable equilibrium, the control torque specified by (5) cannot compel the controlled rotational system to execute a 2π -rad rotation and thus converge to the stable equilibrium point, which prevents global asymptotic stability in $\mathcal{SO}(3)$ from being enforced. In fact, it can be shown that it is impossible to ensure global asymptotic stability with a continuous control law in this case [20], [21]. In practice, however, the CL dynamics are expected to behave as a globally asymptotically stable system because any disturbance, large or small, would move the state away from the unstable equilibrium.

Another relevant observation regarding the CL system resulting from using the law specified by (5) is that the effect of the proportional term, $Jk_\Theta \mathbf{n}_e$, greatly diminishes as the instantaneous CL AEQ moves away from the CL equilibrium AEQ, for rotational errors larger than π rad, because of the $\sin \frac{\Theta_e}{2}$ factor in $\mathbf{n}_e = \mathbf{u}_e \sin \frac{\Theta_e}{2}$. From simple inspection, it is clear that the proportional control effort is close to minimal when the system state is close to the unstable CL equilibrium AEQ (corresponding to a rotational error about the Euler axis close to 2π rad), is maximum halfway between the stable and unstable equilibrium AEQs (corresponding to a rotational error about the Euler axis of π rad), and is minimal at the stable equilibrium point (corresponding to a rotational error about the Euler axis close to 0 rad). These observations regarding the dynamic behavior induced by the law specified by (5) prompted us to introduce a new attitude control approach, which we present in Section III.

III. TWO NEW AXIS-ANGLE ATTITUDE CONTROL LAWS

A. Controller Synthesis and Implementation

A basic heuristic guideline for feedback-controller synthesis is to formulate a control law that increases the actuation effort as the control error grows [22], [23], while ensuring the stability and robust performance of the resulting CL dynamics. Following this design philosophy to address the issues discussed in Section II regarding quaternion-based attitude controllers, we propose a new type of attitude control law—to be integrated into the scheme shown in Fig. 2 for real-time implementation—with the form

$$\boldsymbol{\tau}_j = \mathbf{J} [k_\Theta \mathbf{p}_{e,j} + \mathbf{k}_\omega \boldsymbol{\omega}_e + \boldsymbol{\omega}_d] + \boldsymbol{\omega} \times \mathbf{J} \boldsymbol{\omega}, \quad (6)$$

where the vector $\mathbf{p}_{e,j}$, for $j \in \mathbb{Z}_{>0}$, is defined by scaling the Euler axis associated with \mathbf{q}_e by a class \mathcal{K} function of Θ_e over the operational range $[0, 2\pi]$. In this paper, we consider two functions,

$$\mathbf{p}_{e,1} = \mathbf{u}_e \frac{\Theta_e}{2} \quad \text{and} \quad \mathbf{p}_{e,2} = 2\mathbf{u}_e \sin \frac{\Theta_e}{4}. \quad (7)$$

Similarly to \mathbf{n}_e , the generic *scaled Euler axis* (SEA), $\mathbf{p}_{e,j}$, represents the direction about which the controlled rotational system must rotate to align \mathcal{B} with \mathcal{B}_d . The rationale behind selecting $\mathbf{p}_{e,1}$ is that the term scaling \mathbf{u}_e is directly proportional to the Euler-axis rotational error, Θ_e , and therefore the proportional control effort strictly increases with Θ_e . This approach, however, can lead to actuator saturation; for example, the quadrotor shown in Fig. 1 exhibits a measured thrust-to-weight ratio of only 2.4, which implies that

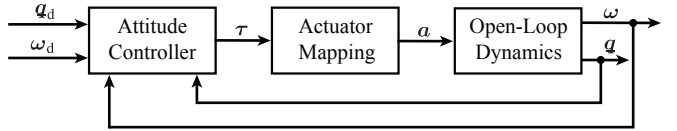


Fig. 2. Block diagram of the upper-level attitude control scheme considered in this paper. In this scheme, the attitude controller receives as inputs the desired attitude quaternion, \mathbf{q}_d ; the desired angular velocity, $\boldsymbol{\omega}_d$; the measured attitude quaternion, \mathbf{q} ; and, the measured angular velocity, $\boldsymbol{\omega}$. Using these inputs, at any given instant, it computes the control torque, $\boldsymbol{\tau} \in \{\boldsymbol{\tau}_b, \boldsymbol{\tau}_1, \boldsymbol{\tau}_2\}$. The actuator mapping receives as its input $\boldsymbol{\tau}$ and generates as its output the vector signal \mathbf{a} that excites the actuators of the open-loop dynamics of the controlled rotational system.

high-gain control laws almost certainly induce saturation of the rotor motors.

Avoiding saturation is the main motivation for selecting the form of $\mathbf{p}_{e,2}$, which generates an increasing control effort as the Euler-axis rotational error, Θ_e , increases within the operational range $[0, 2\pi]$, while reducing the likelihood of the system's actuators exceeding their operational limits. To see these advantages of $\mathbf{p}_{e,2}$ with respect to $\mathbf{p}_{e,1}$, note that the scaling factor in $\boldsymbol{\tau}_2$ is nonlinear in Θ_e with a decreasing slope within the operational range $[0, 2\pi]$. Accordingly, both laws, $\boldsymbol{\tau}_1$ and $\boldsymbol{\tau}_2$, generate similar control torques at small values of Θ_e , but the law that specifies $\boldsymbol{\tau}_2$ produces smaller control torques for relatively large values of Θ_e . The selection of $\sin \frac{\Theta_e}{4}$ in the definition of $\mathbf{p}_{e,2}$ was inspired by attitude control laws based on the *modified Rodrigues parameters* (MRPs) [24]—in which the SEA vector is defined as $\mathbf{u}_e \tan \frac{\Theta_e}{4}$. Note, however, that even though MRPs-based laws also generate an increasing control effort as the system state moves away from the stable CL equilibrium, the value of $\tan \frac{\Theta_e}{4}$ grows unbounded as Θ_e approaches 2π rad, which could be highly problematic in real-time applications. In contrast, $\mathbf{p}_{e,2}$ is well defined for any value of Θ_e . The inclusion of the scalars $\frac{1}{2}$ and 2 in the respective formulations of $\mathbf{p}_{e,1}$ and $\mathbf{p}_{e,2}$ makes all three considered control laws— $\boldsymbol{\tau}_b$, $\boldsymbol{\tau}_1$, and $\boldsymbol{\tau}_2$ —comparable when the system operates near the stable CL equilibrium AEQ.

B. Equilibria of the Two Closed-Loop Systems

Directly from substituting (6) and the left side of (7) into (1), it can be determined that the state-space representation of the CL rotational dynamics corresponding to the control torque $\boldsymbol{\tau}_1$ is given by

$$\begin{aligned} \dot{\mathbf{q}}_e &= \frac{1}{2} \begin{bmatrix} 0 \\ \boldsymbol{\omega}_e \end{bmatrix} \otimes \mathbf{q}_e, \\ \dot{\boldsymbol{\omega}}_e &= - \left[k_\Theta \mathbf{u}_e \frac{\Theta_e}{2} + k_\omega \boldsymbol{\omega}_e \right], \end{aligned} \quad (8)$$

where $\frac{\Theta_e}{2}$ is class \mathcal{K} on $[0, \infty)$ and, as a design restriction, $\Theta_e \in [0, 2\pi]$ rad. As explained in Section III-C, it can be shown that for $k_\Theta, k_\omega \in \mathbb{R}_{>0}$, the unique fixed point of this system is uniformly asymptotically stable. Consequently, an interpretation of this state-space representation is that it describes the dynamics of the deviation from the attitude and angular-velocity references, \mathbf{q}_d and $\boldsymbol{\omega}_d$, and by enforcing asymptotic stability of the CL fixed point, we ensure that $\lim_{t \rightarrow \infty} \mathbf{q} = \mathbf{q}_d$ and $\lim_{t \rightarrow \infty} \boldsymbol{\omega} = \boldsymbol{\omega}_d$. An important additional characteristic of the system specified by (8) is that its RHS is discontinuous and, therefore, not

Lipschitz continuous, which implies that a continuously differentiable solution does not exist [22]. Discontinuities occur at $\Theta_e \in \{2\pi, 4\pi, 6\pi, \dots\} = 2\pi\ell$, for $\ell \in \mathbb{Z}_{>0}$, as \mathbf{u}_e instantaneously switches sign at those values of Θ_e . However, similarly to the case presented in [8], using Carathéodory's concept of solution presented in [25], it can be shown that an absolutely continuous function $s : I \rightarrow \mathcal{S}^3 \times \mathbb{R}^3$ satisfying (8) for almost every time $t \in I \subset \mathbb{R}_{\geq 0}$ exists.

To find the fixed point(s) of the system specified by (8), we set $\dot{\mathbf{q}}_e = [0 \ 0 \ 0]^T$ and $\dot{\boldsymbol{\omega}}_e = [0 \ 0 \ 0]^T$, and solve for \mathbf{q}_e and $\boldsymbol{\omega}_e$. Accordingly, we start with

$$\begin{aligned} -\frac{1}{2}\mathbf{n}_e^T \boldsymbol{\omega}_e &= 0, \\ -\frac{1}{2}[\mathbf{n}_e \times \boldsymbol{\omega}_e - m_e \boldsymbol{\omega}_e] &= \mathbf{0}_{3 \times 1}, \\ -\left[k_\Theta \mathbf{u}_e \frac{\Theta_e}{2} + k_\omega \boldsymbol{\omega}_e\right] &= \mathbf{0}_{3 \times 1}, \end{aligned} \quad (9)$$

and first notice that for the second equation to be satisfied, both vectors $\mathbf{n}_e \times \boldsymbol{\omega}_e$ and $m_e \boldsymbol{\omega}_e$ must be zero because they are orthogonal, which follows directly from the definition of cross product. For the first term in the second line to be zero, one of the following three propositions must hold: (i) \mathbf{n}_e and $\boldsymbol{\omega}_e$ are parallel; (ii) \mathbf{n}_e and $\boldsymbol{\omega}_e$ are both zero; (iii) either \mathbf{n}_e or $\boldsymbol{\omega}_e$ is zero. For the first equation to be satisfied, either (ii) or (iii) is true, or \mathbf{n}_e and $\boldsymbol{\omega}_e$ are orthogonal. Since \mathbf{n}_e and $\boldsymbol{\omega}_e$ cannot be simultaneously orthogonal and parallel, the only feasible option is either (ii) or (iii). Last, from simple examination of the third line, assuming $k_\Theta, k_\omega \in \mathbb{R}_{>0}$, it can be determined that if $\boldsymbol{\omega}_e = \mathbf{0}$, the only possibility to satisfy this last relationship is to have $\Theta_e = 0$, because \mathbf{u}_e is a unit vector ($\mathbf{u}_e \neq \mathbf{0}$). Consistent with this argument, if $\Theta_e = 0$, the only possibility is to have $\boldsymbol{\omega}_e = \mathbf{0}$. Therefore, noticing that $\Theta_e = 0$ implies that $\mathbf{q}_e = [+1 \ 0 \ 0 \ 0]^T$, we conclude that the unique solution to (9) and, therefore, the only fixed point of the CL system specified by (8)—using AEQ representation—is the pair $\{\mathbf{q}_e^* = [+1 \ 0 \ 0 \ 0]^T, \boldsymbol{\omega}_e^* = [0 \ 0 \ 0]^T\}$. As mentioned in Section II and discussed in [26], if a time-invariant continuous CL vector field on $\mathcal{SO}(3)$ has at least one isolated equilibrium, then it cannot be the only one; there must be at least two in order to satisfy Poincaré–Hopf theorem [27]. However, discontinuous feedback laws can be used in attitude control to enforce the existence of a unique CL fixed point and achieve global stabilization on $\mathcal{SO}(3)$. Consistently, the discontinuity of the CL dynamics specified by (8) makes it is possible to have a unique fixed point in similar fashion to the cases discussed in [8] and references therein.

Once more, directly from substituting (6) and the RHS of (7) into (1), it can be determined that the state-space representation of the CL rotational dynamics corresponding to the control torque τ_2 , as specified by (6), is given by

$$\begin{aligned} \dot{\mathbf{q}}_e &= \frac{1}{2} \begin{bmatrix} 0 \\ \boldsymbol{\omega}_e \end{bmatrix} \otimes \mathbf{q}_e, \\ \dot{\boldsymbol{\omega}}_e &= -\left[2k_\Theta \mathbf{u}_e \sin \frac{\Theta_e}{4} + k_\omega \boldsymbol{\omega}_e\right], \end{aligned} \quad (10)$$

in which $\sin \frac{\Theta_e}{4}$ is class \mathcal{K} on $[0, 2\pi]$ and, as a design restriction, $\Theta_e \in [0, 2\pi)$ rad. This design constraint is imposed to make coincide the range of operation with that over

which $\sin \frac{\Theta_e}{4}$ is class \mathcal{K} . As in the case specified by (8), to find the equilibrium point(s) of the state-space representation specified by (10), we set $\dot{\mathbf{q}}_e = [0 \ 0 \ 0 \ 0]^T$ and $\dot{\boldsymbol{\omega}}_e = [0 \ 0 \ 0]^T$ and solve for \mathbf{q}_e and $\boldsymbol{\omega}_e$. Accordingly, we start with

$$\begin{aligned} -\frac{1}{2}\mathbf{n}_e^T \boldsymbol{\omega}_e &= 0, \\ -\frac{1}{2}[\mathbf{n}_e \times \boldsymbol{\omega}_e - m_e \boldsymbol{\omega}_e] &= \mathbf{0}_{3 \times 1}, \\ -\left[2k_\Theta \mathbf{u}_e \sin \frac{\Theta_e}{4} + k_\omega \boldsymbol{\omega}_e\right] &= \mathbf{0}_{3 \times 1}, \end{aligned} \quad (11)$$

and first notice that the analysis for the first two equations is identical to that performed for (8) and (9). From simple examination of the third line, assuming $k_\Theta, k_\omega \in \mathbb{R}_{>0}$, it can be determined that $\boldsymbol{\omega}_e = \mathbf{0}$ if and only if $\Theta_e = 4\pi\ell$, with $\ell \in \mathbb{Z}$, because \mathbf{u}_e is a unit vector ($\mathbf{u}_e \neq \mathbf{0}$). Therefore, over $[0, \infty)$ and the restricted range $[0, 2\pi)$ rad, we conclude that the only equilibrium point of the CL system specified by (10) is the pair $\{\mathbf{q}_e^* = [+1 \ 0 \ 0 \ 0]^T, \boldsymbol{\omega}_e^* = [0 \ 0 \ 0]^T\}$. This finding does not contradict the Poincaré–Hopf theorem—which states that a continuous time-invariant CL vector field on $\mathcal{SO}(3)$ cannot have only one isolated equilibrium [27]—because the dynamics specified by (10) are discontinuous at $\Theta_e \in \{2\pi, 6\pi, 10\pi, \dots\} = 2\pi(2\ell + 1)$, for $\ell \in \mathbb{Z}_{\geq 0}$. Furthermore, note that these discontinuities lie outside the selected range of operation, $[0, 2\pi)$.

C. Stability Analysis

The stability of the equilibrium $\{\mathbf{q}_e^*, \boldsymbol{\omega}_e^*\}$ corresponding to the CL system specified by (8) can be analyzed by invoking *Lyapunov's direct method* as stated in Theorem 4.9 of [22]. We state this result in the form of a proposition.

Proposition 1. *Let the attitude and angular-velocity references, \mathbf{q}_d and $\boldsymbol{\omega}_d$, be smooth and bounded functions of time, and let k_Θ and k_ω be constant positive scalars. Then, the fixed point $\{\mathbf{q}_e^*, \boldsymbol{\omega}_e^*\}$, with $\mathbf{q}_e^* = [+1 \ 0 \ 0 \ 0]^T$ and $\boldsymbol{\omega}_e^* = [0 \ 0 \ 0]^T$, of the CL state-space representation of the rotational dynamics specified by (8) is uniformly asymptotically stable.*

Proof. We start by defining

$$V_1 = \frac{1}{2}k_\Theta^{-1}\boldsymbol{\omega}_e^T \boldsymbol{\omega}_e + \frac{1}{4}\Theta_e^2 + c(\mathbf{n}_e^T \mathbf{n}_e + \mathbf{n}_e^T \boldsymbol{\omega}_e), \quad (12)$$

in which $c \in \mathbb{R}_{>0}$. It can be shown that V_1 meets the conditions specified in [22] for a *Lyapunov function* (LF) because \mathbf{q}_d and $\boldsymbol{\omega}_d$ are smooth functions of time. Specifically, by imposing this property on the attitude and angular-velocity references, we ensure that V_1 is continuously differentiable in the selected range of operation, $\Theta_e \in [0, 2\pi)$ rad, and when we substitute $\{\mathbf{q}_e^*, \boldsymbol{\omega}_e^*\}$ into (12), we obtain that $V_1(\mathbf{q}_e^*, \boldsymbol{\omega}_e^*) = 0$. Furthermore, V_1 can be lower bounded according to

$$\begin{aligned} V_1 &\geq \frac{1}{2}k_\Theta^{-1}\|\boldsymbol{\omega}_e\|_2^2 + c\|\mathbf{n}_e\|_2^2 - c\|\mathbf{n}_e\|_2\|\boldsymbol{\omega}_e\|_2 \\ &= \mathbf{x}_e^T \mathbf{P} \mathbf{x}_e \geq \lambda_{\min}\{\mathbf{P}\} \|\mathbf{x}_e\|_2^2, \end{aligned} \quad (13)$$

where

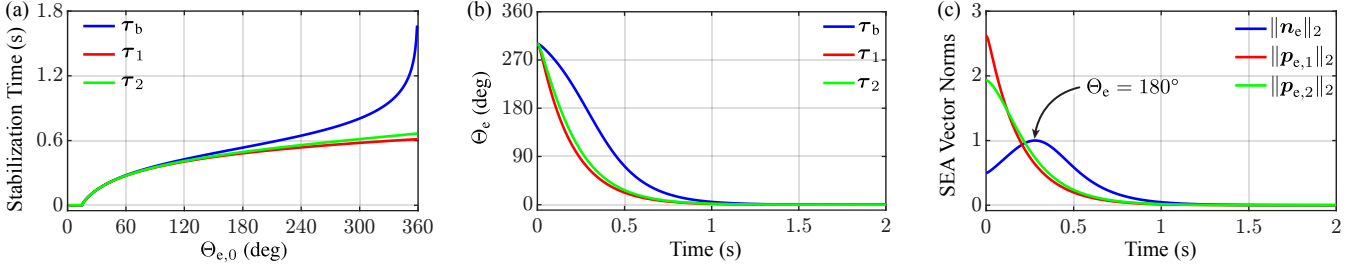


Fig. 3. Simulation results. (a) Stabilization times versus the initial Euler-axis rotational error, $\Theta_{e,0}$, obtained using the three tested attitude control laws, τ_b , τ_1 , and τ_2 . (b) Regulation responses of the Euler-axis rotational errors, $\Theta_e(t)$, for $t \in [0, 2]$ s and initial condition $\Theta_{e,0} = 300^\circ$, obtained using the three tested control laws, τ_b , τ_1 , and τ_2 . (c) SEA vector norms— $\|n_e\|_2$, $\|p_{e,1}\|_2$, and $\|p_{e,2}\|_2$ —corresponding to the flight cases in (b), evolving over time within the range $[0, 2]$ s.

$$\begin{aligned} x_e &= [\|n_e\|_2 \ \|\omega_e\|_2]^T \\ \text{and} \\ P &= \begin{bmatrix} c & -\frac{1}{2}c \\ -\frac{1}{2}c & \frac{1}{2}k_\Theta^{-1} \end{bmatrix} \succ \mathbf{0}, \end{aligned} \quad (14)$$

for a value of c sufficiently small, thus making V_1 strictly positive for any $x_e \neq \mathbf{0}$.

Next, taking the time derivative of V_1 in (12) yields

$$\begin{aligned} \dot{V}_1 &= -p_{e,1}^T \omega_e - k_\Theta^{-1} k_\omega \omega_e^T \omega_e + \frac{1}{2} \dot{\Theta}_e \Theta_e \\ &\quad + 2c \dot{n}_e^T n_e + c \dot{n}_e^T \omega_e + c n_e^T \dot{\omega}_e, \end{aligned} \quad (15)$$

which—following the analysis in Appendix A—can be upper bounded according to

$$\begin{aligned} \dot{V}_1 &\leq -k_\Theta^{-1} k_\omega \|\omega_e\|_2^2 + c \|\omega_e\|_2 \|n_e\|_2 \\ &\quad + \frac{1}{2} c \|\omega_e\|_2^2 - c k_\Theta \|n_e\|_2^2 + c k_\omega \|\omega_e\|_2 \|n_e\|_2 \\ &= -x_e^T Q x_e \leq -\lambda_{\min}\{Q\} \|x_e\|_2^2, \end{aligned} \quad (16)$$

with

$$Q = \begin{bmatrix} c k_\Theta & -\frac{1}{2}c(k_\omega + 1) \\ -\frac{1}{2}c(k_\omega + 1) & k_\Theta^{-1} k_\omega - \frac{1}{2}c \end{bmatrix} \succ \mathbf{0}, \quad (17)$$

for a value of c sufficiently small, thus making \dot{V}_1 strictly negative for any $x_e \neq \mathbf{0}$.

Hence, we conclude that the unique CL equilibrium of the state-space representation specified by (8), $\{q_e^*, \omega_e^*\}$ is uniformly asymptotically stable. \square

Next, we analyze and prove the stability of the equilibrium $\{q_e^*, \omega_e^*\}$ corresponding to the CL system specified by (10), also invoking *Lyapunov's direct method* as stated in Theorem 4.9 of [22]. We state this result in the form of a proposition.

Proposition 2. *Let the attitude and angular-velocity references, q_d and ω_d , be smooth and bounded functions of time, and let k_Θ and k_ω be constant positive scalars. Then, the fixed point $\{q_e^*, \omega_e^*\}$, with $q_e^* = [+1 \ 0 \ 0 \ 0]^T$ and $\omega_e^* = [0 \ 0 \ 0]^T$, of the CL state-space representation of the rotational dynamics given by (10) is uniformly asymptotically stable inside the range of operation, $\Theta_e \in [0, 2\pi]$ rad.*

Proof. We start by defining

$$V_2 = \frac{1}{2} k_\Theta^{-1} \omega_e^T \omega_e + 16 \sin^2 \frac{\Theta_e}{8} + c n_e^T n_e + c n_e^T \omega_e, \quad (18)$$

in which $c \in \mathbb{R}_{>0}$. It can be shown that V_2 meets the conditions specified in [22] for an LF because q_d and ω_d are smooth functions of time. Specifically, by imposing this property on the attitude and angular-velocity references, we ensure that V_2 is continuously differentiable, and when we substitute $\{q_e^*, \omega_e^*\}$ into (18), we obtain that $V_2(q_e^*, \omega_e^*) = 0$. Furthermore, V_2 can be lower bounded according to

$$\begin{aligned} V_2 &\geq \frac{1}{2} k_\Theta^{-1} \|\omega_e\|_2^2 + c \|n_e\|_2^2 - c \|n_e\|_2 \|\omega_e\|_2 \\ &= x_e^T P x_e \geq \lambda_{\min}\{P\} \|x_e\|_2^2, \end{aligned} \quad (19)$$

for a value of c sufficiently small to make V_2 strictly positive for any $x_e \neq \mathbf{0}$. In (19), both x_e and P have exactly the same form specified in (14). Next, taking the time derivative of V_2 defined by (18) yields

$$\begin{aligned} \dot{V}_2 &= -p_{e,2}^T \omega_e - k_\Theta^{-1} k_\omega \omega_e^T \omega_e + 32 \frac{\dot{\Theta}_e}{8} \sin \frac{\Theta_e}{8} \cos \frac{\Theta_e}{8} \\ &\quad + 2c \dot{n}_e^T n_e + c \dot{n}_e^T \omega_e + c n_e^T \dot{\omega}_e, \end{aligned} \quad (20)$$

which—following the analysis in Appendix B—can be upper bounded according to

$$\begin{aligned} \dot{V}_2 &\leq -k_\Theta^{-1} k_\omega \|\omega_e\|_2^2 + c \|\omega_e\|_2 \|n_e\|_2 \\ &\quad + \frac{1}{2} c \|\omega_e\|_2^2 - c k_\Theta \|n_e\|_2^2 + c k_\omega \|\omega_e\|_2 \|n_e\|_2 \\ &= -x_e^T Q x_e \leq -\lambda_{\min}\{Q\} \|x_e\|_2^2, \end{aligned} \quad (21)$$

with Q defined exactly as in (17), for a value of c sufficiently small to make \dot{V}_2 strictly negative for any $x_e \neq \mathbf{0}$.

Hence, we conclude that the unique CL equilibrium of the state-space representation specified by (10), $\{q_e^*, \omega_e^*\}$, is uniformly asymptotically stable. \square

IV. SIMULATIONS AND EXPERIMENTS

A. Numerical Simulations

To first assess and demonstrate the functionality and performance of the two attitude control laws specified by (6) and (7), we compared them with the benchmark law specified by (5) through numerical simulations implemented and run on Simulink 23.2 (MATLAB R2023b), using the Dormand-Prince algorithm with a fixed step size of 10^{-4} s. We set and initialized the simulations using the parameters of the Crazyflie 2.1 [28]—shown in Fig. 1—and empirically-selected controller gains that satisfy the stability conditions discussed in Section III. Accordingly, we selected $J = \text{diag}\{16.57, 16.66, 29.26\} \cdot 10^{-6} \text{ kg} \cdot \text{m}^2$, $k_\Theta = 1000 \text{ N} \cdot \text{m}$, and $k_\omega = 100 \text{ N} \cdot \text{m} \cdot \text{s} \cdot \text{rad}^{-1}$. It can be

verified that for these controller gains, a value $c \leq 10^{-3}$ makes \mathbf{P} and \mathbf{Q} positive definite. For each control law— τ_b , τ_1 , and τ_2 —we simulated 359 tumble-recovery maneuvers during which the flier is commanded to stabilize itself from an upended flight position to reach the desired state given by the pair $\{\mathbf{q}_d = [+1 \ 0 \ 0 \ 0]^T, \boldsymbol{\omega}_d = [0 \ 0 \ 0]^T\}$. Specifically, each simulation was initialized at a time t_0 with an Euler axis of rotation, $\mathbf{u}_0 = \mathbf{u}(t_0)$, generated randomly with a new seed using MATLAB. The initial rotation about the Euler axis, $\Theta_0 = \Theta(t_0)$, was sequentially selected from 1 to 359° for each new simulation in increments of 1° , and the initial angular velocity, $\boldsymbol{\omega}_0 = \boldsymbol{\omega}(t_0)$, was set to zero for all the simulated cases. To evaluate and compare the controllers, we use as a figure of merit the *stabilization time*, defined as the time it takes for the rotation error, Θ_e , about the attitude-error Euler axis, \mathbf{u}_e , to reach a value lower than 15° .

Fig. 3(a) shows the stabilization times corresponding to the three simulated control laws as functions of the initial rotation error, $\Theta_{e,0} = \Theta_e(t_0)$. As seen, the results corresponding to the three different controllers are very similar for $\Theta_{e,0} \leq 180^\circ$; however, the superior performance of laws τ_1 and τ_2 , relative to that corresponding to the quaternion-based τ_b , becomes evident for cases in which $\Theta_{e,0} > 180^\circ$. For example, for values of $\Theta_{e,0} > 350^\circ$, the stabilization time achieved with τ_b is more than 2 times higher than those achieved with the two laws introduced and studied in this paper. This difference in performance can be critical in situations in which the controlled system must recover from an unexpected disturbance that significantly changed its attitude. Furthermore, regarding design, functionality, and performance, it is important to note that τ_1 and τ_2 were conceived to be implemented as constituents of switching control schemes such as those presented in [1]–[3]. Consequently, the rationale behind testing cases in which $\Theta_{e,0} > 180^\circ$ is that, in some cases during flight, it is expected the switching controller to apply the proportional torque component in the direction of the longest rotational-error path.

Figs. 3(b) and (c) show the simulated regulation responses of the rotation error, $\Theta_e(t)$, for $t \in [0, 2]$ s, about the attitude-error Euler axis, and the SEA vector norms— $\|\mathbf{n}_e\|_2$, $\|\mathbf{p}_{e,1}\|_2$, and $\|\mathbf{p}_{e,2}\|_2$ —in the proportional terms of the three compared laws— τ_b , τ_1 , and τ_2 —for $\Theta_{e,0} = 300^\circ$. Simple inspection of Fig. 3(b) allows us to determine that the stabilization time in the quaternion-based control case is significantly higher than in the τ_1 -based and τ_2 -based cases; 0.80 s versus 0.58 and 0.61 s, respectively. The data in Fig. 3(c) confirms that the effect sought with the introduction of the two laws specified by (6) and (7) is fully accomplished as the proportional control effort applied to the rotational system at $\Theta_e = 300^\circ$ is about more than three and two times those corresponding to τ_1 and τ_2 , respectively. Furthermore, both $\|\mathbf{p}_{e,1}\|_2$ and $\|\mathbf{p}_{e,2}\|_2$ decrease as Θ_e decreases from 300 to 0° . In contrast, it can be observed that the magnitude of $\|\mathbf{n}_e\|_2$ increases as Θ_e decreases from 300 to 180° to rapidly decrease after passing this point. This dynamical behavior is inconsistent with the notion that *the actuation effort should grow with the magnitude of the control error*.

The simulated maneuvers presented in this section were selected to demonstrate and highlight the differences between the two new control laws—specified by (6) and (7)—and the quaternion-based law used as benchmark—specified by

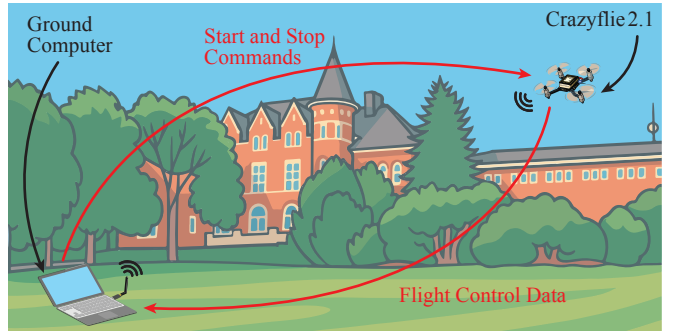


Fig. 4. Experimental setup used during the performance of flight control tests. All the experiments were performed outdoor using a ground computer equipped with a Crazyradio 2.0 dongle, which sends the initialization and stop commands for the execution of controlled flight maneuvers. Also, during flight, the flier—a Crazyflie 2.1—sends its instantaneous state to the ground computer for data collection.

(5). By choosing an initial condition of the rotation error, $\Theta_{e,0}$, about the attitude-error Euler axis larger than 180° , the CL AEQ of the attitude dynamics resulting from using (5) lies very close to the unstable CL equilibrium AEQ and, therefore, as explained in Section II, the proportional control effort takes values significantly lower than the maximum achievable. In contrast, by design, the two new control laws always generate a proportional driving torque that increases with Θ_e . A last interesting observation regarding the simulation results summarized in Fig. 3 is that the time evolutions of Θ_e corresponding to τ_1 and τ_2 look very similar. The values of $\|\mathbf{p}_{e,1}\|_2$ and $\|\mathbf{p}_{e,2}\|_2$, however, look very different at large magnitudes of Θ_e . The relatively high values of $\|\mathbf{p}_{e,1}\|_2$ at high values of Θ_e might lead to actuator saturation depending on the characteristics of the controlled rotational system. For this reason, for the real-time flight control experiments presented next, we implemented τ_b and τ_2 only, considering the limited thrust-to-weight of the tested quadrotor, i.e., 2.4.

B. Real-Time Flight Tests

To compare the dynamical behavior of the two tested attitude control laws, τ_b and τ_2 , in real time, we implemented each of them as a constituent of the model-predictive switching scheme described in [1], using the quadrotor shown in Fig. 1 with the same controller parameters specified in Section IV-A. As depicted in Fig. 4, we performed flight tests outdoor using a ground computer equipped with the Crazyradio 2.0 dongle. During an experiment, this ground system sends initialization and stop commands for executing maneuvers, and collects the flight data sent from the drone to the ground computer through radio communication at a rate of 100 Hz. The executed flight tests were conceived to emulate high-speed tumble-recovery maneuvers resulting from *throw launches*—expected to be used in military, or search and rescue scenarios—consisting of two phases. During the first phase, the quadrotor is thrown by the experimenter in the air with an unknown relatively high angular velocity while the controller and rotors remain off. During the second phase, the controller is activated and the rotors are turned on in order to stabilize the quadrotor's attitude and reach a desired hovering state given by the pair $\{\mathbf{q}_d = [+1 \ 0 \ 0 \ 0]^T, \boldsymbol{\omega}_d = [0 \ 0 \ 0]^T\}$. The quadrotor executes

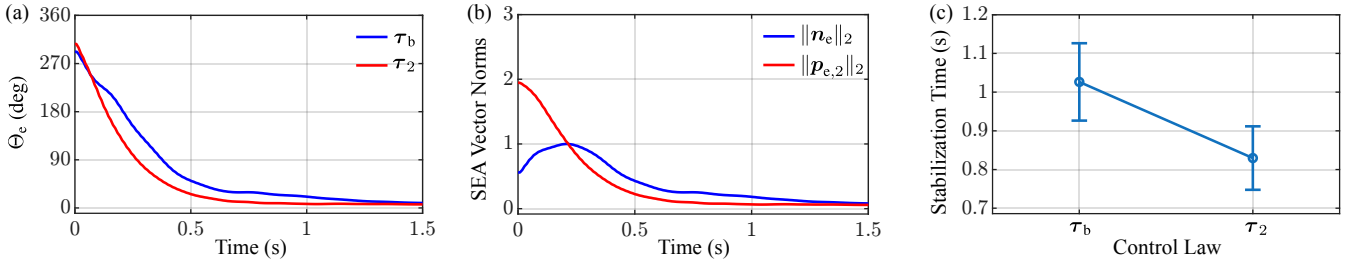


Fig. 5. Experimental results. (a) Time evolutions of the Euler-axis rotational errors, $\Theta_e(t)$, for $t \in [0, 1.5]$ s, obtained using the benchmark attitude control law, τ_b , and the new attitude control law, τ_2 . (b) SEA vector norms— $\|n_e\|_2$, $\|p_{e,1}\|_2$, and $\|p_{e,2}\|_2$ —corresponding to the flight cases in (a), evolving over time within the range [0, 1.5] s. (c) Mean and SEM of the stabilization times corresponding to 25 back-to-back experiments respectively performed using τ_b and τ_2 .

the entire maneuver autonomously, using onboard sensing and computation only, with the attitude controller running at a frequency of 500 Hz.

Fig. 5(a) shows the time evolution of Θ_e measured during two experiments correspondingly performed using τ_b and τ_2 , and initialized with similar initial conditions. In these particular tests, similarly to the simulation cases presented in Section IV-A, the stabilization time corresponding to τ_2 is significantly shorter than that achieved with τ_b —0.63 versus 1.18 s. Fig. 5(b) shows the time evolutions of $\|n_e\|_2$ and $\|p_{e,2}\|_2$. Similarly to the simulation cases presented in Section IV-A, $\|n_e\|_2$ increases as Θ_e decreases from its initial condition until reaching 180° , and decreases after passing this point, thus exhibiting the undesired behavior already discussed in the previous sections. In contrast, $\|p_{e,2}\|_2$ decreases as Θ_e decreases from its initial condition until reaching a value of approximately 0° . Video footage of these experiments can be seen in the accompanying supplementary movie.

Last, in Fig. 5(c), each datum shows the mean and *standard error of the mean* (SEM) of the stabilization times corresponding to 25 back-to-back experiments respectively executed using τ_b (left) and τ_2 (right). As seen, the mean values achieved with τ_b and τ_2 are 1.03 and 0.83 s, respectively. Although the difference between these two values is not pronounced due to actuation limitations of the experimental platform, they are consistent with the simulation data presented in Section IV-A and provide convincing experimental evidence of the superior performance achievable with τ_2 relative to that obtained with τ_b . Furthermore, the SEM values corresponding to τ_b and τ_2 are 0.10 and 0.08 s, respectively, which suggests that the mean value corresponding to τ_2 is a more precise estimate of the stabilization time, used as a measure of performance. A large variability of the data is expected due to the *stochastic* nature of tumble-recovery experiments; in some experiments, the initial Θ_e and ω_e are small, which results in relatively low stabilization times, while in other experiments, the initial Θ_e and ω_e are large, which results in relatively high stabilization times.

V. CONCLUSIONS AND FUTURE RESEARCH

We introduced a new methodology for synthesizing attitude controllers for rotational systems that can be modeled as rigid bodies, such as satellites, drones, and microswimmers. In this approach—in contrast to quaternion-based schemes—the controller is defined using an Euler axis–angle attitude-error law that guarantees the existence of a unique

CL equilibrium AEQ and provides greater flexibility in the use of proportional-control effort. To illustrate the proposed methodology, we defined two different attitude control laws and, for each case studied, we showed that the unique equilibrium of the CL dynamics is uniformly asymptotically stable by constructing a strict Lyapunov function for the system. To test and demonstrate the functionality and performance of the two resulting CL schemes, we conducted hundreds of numerical simulations and executed dozens of real-time flight experiments using a small-sized quadrotor (Crazyflie 2.1). In particular, we studied and discussed tumble-recovery maneuvers controlled by the three controllers—the two new ones and a benchmark—presented in this paper. The obtained simulation and experimental results provide compelling evidence for the suitability of the new control schemes, which can be particularly useful as constituents of switching architectures that account for the angular velocity when selecting the direction in which proportional torque is applied. Currently, controllers of this type do not account for actuator saturation, which is a matter of ongoing and future research at the *Autonomous Microrobotic Systems Laboratory* (AMSL).

REFERENCES

- [1] F. M. F. R. Gonçalves, R. M. Bena, K. I. Matveev, and N. O. Pérez-Arcanibia, “MPS: A New Method for Selecting the Stable Closed-Loop Equilibrium Attitude-Error Quaternion of a UAV During Flight,” in *Proc. IEEE Int. Conf. Robot. Autom. (ICRA)*, Yokohama, Japan, May 2024, pp. 8363–8369.
- [2] ———, “A Lyapunov-Based Switching Scheme for Selecting the Stable Closed-Loop Fixed Attitude-Error Quaternion During Flight,” in *Proc. 7th Iberian Robot. Conf. (ROBOT)*, Madrid, Spain, Nov. 2024, 8 pp.
- [3] F. M. F. R. Gonçalves, R. M. Bena, and N. O. Pérez-Arcanibia, “Closed-Loop Stability of a Lyapunov-Based Switching Scheme for Energy-Efficient Torque-Input-Selection During Flight,” in *Proc. IEEE Int. Conf. Robot. Biomim. (ROBIO)*, Bangkok, Thailand, Dec. 2024, pp. 1941–1947.
- [4] R. M. Bena, X.-T. Nguyen, X. Yang, A. A. Calderón, Y. Chen, and N. O. Pérez-Arcanibia, “A Multiplatform Position Control Scheme for Flying Robotic Insects,” *J. Intell. Robot. Syst.*, vol. 105, no. 1, May 2022, Art. no. 19.
- [5] R. M. Bena, X. Yang, A. A. Calderón, and N. O. Pérez-Arcanibia, “High-Performance Six-DOF Flight Control of the Bee++: An Inclined-Stroke-Plane Approach,” *IEEE Trans. Robot.*, vol. 39, no. 2, pp. 1668–1684, Apr. 2023.
- [6] C. G. Mayhew, R. G. Sanfelice, and A. R. Teel, “Robust Global Asymptotic Attitude Stabilization of a Rigid Body by Quaternion-Based Hybrid Feedback,” in *Proc. IEEE Conf. Decis. Control (CDC)*, Chin. Control Conf. (CCC), Shanghai, China, Dec. 2009, pp. 2522–2527.
- [7] ———, “On Quaternion-Based Attitude Control and the Unwinding Phenomenon,” in *Proc. Amer. Control Conf. (ACC)*, San Francisco, CA, USA, Jun. 2011, pp. 299–304.
- [8] ———, “Quaternion-Based Hybrid Control for Robust Global Attitude Tracking,” *IEEE Trans. Autom. Control*, vol. 56, no. 11, pp. 2555–2566, Nov. 2011.

[9] B. Pratama, A. Muis, A. Subiantoro, M. Djemai, and R. B. Atitallah, “Quadcopter Trajectory Tracking and Attitude Control Based on Euler Angle Limitation,” in *Proc. 6th Int. Conf. Control Eng. Inf. Technol. (CEIT)*, Istanbul, Turkey, Oct. 2018, 6 pp.

[10] A. Mokhtari and A. Benallegue, “Dynamic Feedback Controller of Euler Angles and Wind Parameters Estimation for a Quadrotor Unmanned Aerial Vehicle,” in *Proc. IEEE Int. Conf. Robot. Autom. (ICRA)*, New Orleans, LA, USA, Apr. 2004, pp. 2359–2366.

[11] C. W. Kang and C. G. Park, “Euler Angle Based Attitude Estimation Avoiding the Singularity Problem,” in *Proc. 18th IFAC World Cong. (IFAC’11)*, Milan, Italy, Aug. 2011, pp. 2096–2102.

[12] T. Lee, “Geometric Tracking Control of the Attitude Dynamics of a Rigid Body on $SO(3)$,” in *Proc. Amer. Control Conf. (ACC)*, San Francisco, CA, USA, Jun. 2011, pp. 1200–1205.

[13] ———, “Geometric Control of Quadrotor UAVs Transporting a Cable-Suspended Rigid Body,” *IEEE Trans. Autom. Control*, vol. 26, no. 1, pp. 255–264, Jan. 2018.

[14] G. Wu and K. Sreenath, “Geometric Control of Multiple Quadrotors Transporting a Rigid-body Load,” in *Proc. IEEE Conf. Decis. Control (CDC)*, Los Angeles, CA, USA, Dec. 2014, pp. 6141–6148.

[15] J. Wei, S. Zhang, A. Adaldo, X. Hu, and K. H. Johansson, “Finite-Time Attitude Synchronization With a Discontinuous Protocol,” in *Proc. Int. Conf. Control Autom. (ICCA)*, Ohrid, Macedonia, Jul. 2017, pp. 192–197.

[16] J. Thunberg, W. Song, E. Montijano, Y. Hong, and X. Hu, “Distributed Attitude Synchronization Control of Multi-Agent Systems With Switching Topologies,” *Automatica*, vol. 50, no. 3, pp. 832–840, Mar. 2014.

[17] E. K. Blankenship, C. K. Trygstad, F. M. F. R. Gonçalves, and N. O. Pérez-Arcibbia, “VLEIBot: A New 45-mg Swimming Microrobot Driven by a Bioinspired Anguilliform Propulsor,” in *Proc. IEEE Int. Conf. Robot. Autom. (ICRA)*, Yokohama, Japan, May 2024, pp. 6014–6021.

[18] C. K. Trygstad, C. R. Longwell, F. M. F. R. Gonçalves, and N. O. Pérez-Arcibbia, “A 93-Milligram Submersible Swimmer Driven by Energy-Efficient SMA-Based Millimeter-Scale Actuators,” *npj Robotics*, 2025, to appear.

[19] C. K. Trygstad, C. R. Longwell, F. M. F. R. Gonçalves, E. K. Blankenship, and N. O. Pérez-Arcibbia, “Feedback Control of a Single-Tail Bioinspired 59-mg Swimmer,” in *Proc. IEEE/RSJ Int. Conf. Intell. Robots Syst. (IROS)*, Hangzhou, China, Oct. 2025, pp. 5722–5729.

[20] S. P. Bhat and D. S. Bernstein, “A Topological Obstruction to Continuous Global Stabilization of Rotational Motion and the Unwinding Phenomenon,” *Syst. Control Lett.*, vol. 39, no. 1, pp. 63–70, Jan. 2000.

[21] D. Liberzon, *Switching in Systems and Control*. New York, NY, USA: Springer, 2003.

[22] H. K. Khalil, *Nonlinear Systems*. Upper Saddle River, NJ, USA: Prentice Hall, 2002.

[23] K. Ogata, *Modern Control Engineering*. Upper Saddle River, NJ, USA: Prentice Hall, 2010.

[24] H. Schaub and J. L. Junkins, *Analytical Mechanics of Space Systems*. Reston, VA, USA: AIAA, Inc., 2018.

[25] O. Hájek, “Discontinuous Differential Equations, I,” *J. Differ. Equ.*, vol. 32, no. 2, pp. 149–170, May 1979.

[26] N. A. Chaturvedi, A. K. Sanyal, and N. H. McClamroch, “Rigid-Body Attitude Control,” *IEEE Control Syst. Mag.*, vol. 31, no. 3, pp. 30–51, Jun. 2011.

[27] U. Kalabić, R. Gupta, S. D. Cairano, A. Bloch, and I. Kolmanovsky, “MPC on Manifolds with an Application to $SE(3)$,” in *Proc. Amer. Control Conf. (ACC)*, Boston, MA, USA, Jul. 2016, pp. 7–12.

[28] Bitcraze, <https://www.bitcraze.io/products/crazyflie-2-1/>.

APPENDIX

A. Upper Bound for \dot{V}_1 in Proposition 1

It is easy to verify that the time derivative of V_1 is

$$\begin{aligned} \dot{V}_1 &= -\mathbf{p}_{e,1}^T \boldsymbol{\omega}_e - k_\Theta^{-1} k_\omega \boldsymbol{\omega}_e^T \boldsymbol{\omega}_e + \frac{1}{2} \dot{\Theta}_e \Theta_e + 2c\dot{\mathbf{n}}_e^T \mathbf{n}_e \\ &\quad + c\dot{\mathbf{n}}_e^T \boldsymbol{\omega}_e + c\mathbf{n}_e^T \dot{\boldsymbol{\omega}}_e. \end{aligned} \quad (22)$$

Then, recalling that $\mathbf{p}_{e,1} = \mathbf{u}_e \frac{\Theta_e}{2}$ and $\dot{\Theta}_e = \boldsymbol{\omega}_e^T \mathbf{u}_e$, we can rewrite (22) as

$$\begin{aligned} \dot{V}_1 &= -\frac{1}{2} \mathbf{u}_e^T \boldsymbol{\omega}_e \Theta_e - k_\Theta^{-1} k_\omega \boldsymbol{\omega}_e^T \boldsymbol{\omega}_e + \frac{1}{2} \boldsymbol{\omega}_e^T \mathbf{u}_e \Theta_e \\ &\quad + 2c\dot{\mathbf{n}}_e^T \mathbf{n}_e + c\dot{\mathbf{n}}_e^T \boldsymbol{\omega}_e + c\mathbf{n}_e^T \dot{\boldsymbol{\omega}}_e \\ &= -k_\Theta^{-1} k_\omega \boldsymbol{\omega}_e^T \boldsymbol{\omega}_e + 2c\dot{\mathbf{n}}_e^T \mathbf{n}_e + c\dot{\mathbf{n}}_e^T \boldsymbol{\omega}_e + c\mathbf{n}_e^T \dot{\boldsymbol{\omega}}_e, \end{aligned} \quad (23)$$

in which, directly from (8),

$$\dot{\mathbf{n}}_e = \frac{1}{2} (m_e \boldsymbol{\omega}_e + \boldsymbol{\omega}_e \times \mathbf{n}_e). \quad (24)$$

Next, substituting (24) into (23) and noticing that $\boldsymbol{\omega}_e \times \mathbf{n}_e$ is orthogonal to $\boldsymbol{\omega}_e$ and \mathbf{n}_e , (23) can be further simplified as

$$\dot{V}_1 = -k_\Theta^{-1} k_\omega \boldsymbol{\omega}_e^T \boldsymbol{\omega}_e + c m_e \boldsymbol{\omega}_e^T \mathbf{n}_e + \frac{1}{2} c m_e \boldsymbol{\omega}_e^T \boldsymbol{\omega}_e + c \mathbf{n}_e^T \dot{\boldsymbol{\omega}}_e, \quad (25)$$

which, by using the RHS of the second equation in (8), becomes

$$\begin{aligned} \dot{V}_1 &= -k_\Theta^{-1} k_\omega \boldsymbol{\omega}_e^T \boldsymbol{\omega}_e + c m_e \boldsymbol{\omega}_e^T \mathbf{n}_e + \frac{1}{2} c m_e \boldsymbol{\omega}_e^T \boldsymbol{\omega}_e \\ &\quad - c k_\Theta \mathbf{n}_e^T \mathbf{p}_{e,1} - c k_\omega \mathbf{n}_e^T \boldsymbol{\omega}_e. \end{aligned} \quad (26)$$

This expression can be upper bounded as

$$\begin{aligned} \dot{V}_1 &\leq -k_\Theta^{-1} k_\omega \|\boldsymbol{\omega}_e\|_2^2 + c \|\boldsymbol{\omega}_e\|_2 \|\mathbf{n}_e\|_2 + \frac{1}{2} c \|\boldsymbol{\omega}_e\|_2^2 \\ &\quad - c k_\Theta \|\mathbf{n}_e\|_2^2 + c k_\omega \|\mathbf{n}_e\|_2 \|\boldsymbol{\omega}_e\|_2, \end{aligned} \quad (27)$$

because $-\|\mathbf{n}_e\|_2^2 \geq -\|\mathbf{n}_e\|_2 \|\mathbf{p}_{e,1}\|_2$, for any $\Theta_e \in [0, 2\pi)$ —the operational range selected by design. Last, using matrix manipulation rules, we obtain

$$\dot{V}_1 \leq -\mathbf{x}_e^T \begin{bmatrix} c k_\Theta & -\frac{1}{2} c (k_\omega + 1) \\ -\frac{1}{2} c (k_\omega + 1) & k_\Theta^{-1} k_\omega - \frac{1}{2} c \end{bmatrix} \mathbf{x}_e, \quad (28)$$

where $\mathbf{x}_e = [\|\mathbf{n}_e\|_2 \ \|\boldsymbol{\omega}_e\|_2]^T$.

B. Upper Bound for \dot{V}_2 in Proposition 2

It is easy to verify that the time derivative of V_2 is

$$\begin{aligned} \dot{V}_2 &= -\mathbf{p}_{e,2}^T \boldsymbol{\omega}_e - k_\Theta^{-1} k_\omega \boldsymbol{\omega}_e^T \boldsymbol{\omega}_e + 32 \frac{\dot{\Theta}_e}{8} \sin \frac{\Theta_e}{8} \cos \frac{\Theta_e}{8} \\ &\quad + 2c\dot{\mathbf{n}}_e^T \mathbf{n}_e + c\dot{\mathbf{n}}_e^T \boldsymbol{\omega}_e + c\mathbf{n}_e^T \dot{\boldsymbol{\omega}}_e, \end{aligned} \quad (29)$$

Then, recalling that $\mathbf{p}_{e,2} = 2\mathbf{u}_e \sin(\frac{\Theta_e}{4})$, $\dot{\Theta}_e = \boldsymbol{\omega}_e^T \mathbf{u}_e$, and $\sin \frac{\Theta_e}{8} \cos \frac{\Theta_e}{8} = \frac{1}{2} \sin \frac{\Theta_e}{4}$, we can rewrite (29) as

$$\begin{aligned} \dot{V}_2 &= -2\mathbf{u}_e^T \boldsymbol{\omega}_e \sin \frac{\Theta_e}{4} - k_\Theta^{-1} k_\omega \boldsymbol{\omega}_e^T \boldsymbol{\omega}_e + 2\mathbf{u}_e^T \mathbf{u}_e \sin \frac{\Theta_e}{4} \\ &\quad + 2c\dot{\mathbf{n}}_e^T \mathbf{n}_e + c\dot{\mathbf{n}}_e^T \boldsymbol{\omega}_e + c\mathbf{n}_e^T \dot{\boldsymbol{\omega}}_e \\ &= k_\Theta^{-1} k_\omega \boldsymbol{\omega}_e^T \boldsymbol{\omega}_e + 2c\dot{\mathbf{n}}_e^T \mathbf{n}_e + c\dot{\mathbf{n}}_e^T \boldsymbol{\omega}_e + c\mathbf{n}_e^T \dot{\boldsymbol{\omega}}_e, \end{aligned} \quad (30)$$

in which, directly from (10),

$$\dot{\mathbf{n}}_e = \frac{1}{2} (m_e \boldsymbol{\omega}_e + \boldsymbol{\omega}_e \times \mathbf{n}_e). \quad (31)$$

Next, substituting (31) into (30) and noticing that $\boldsymbol{\omega}_e \times \mathbf{n}_e$ is orthogonal to $\boldsymbol{\omega}_e$ and \mathbf{n}_e , (30) can be further simplified as

$$\dot{V}_2 = -k_\Theta^{-1} k_\omega \boldsymbol{\omega}_e^T \boldsymbol{\omega}_e + c m_e \boldsymbol{\omega}_e^T \mathbf{n}_e + \frac{1}{2} c m_e \boldsymbol{\omega}_e^T \boldsymbol{\omega}_e + c \mathbf{n}_e^T \dot{\boldsymbol{\omega}}_e, \quad (32)$$

which, by using the RHS of the second equation in (10), becomes

$$\begin{aligned} \dot{V}_2 &= -k_\Theta^{-1} k_\omega \boldsymbol{\omega}_e^T \boldsymbol{\omega}_e + c m_e \boldsymbol{\omega}_e^T \mathbf{n}_e + \frac{1}{2} c m_e \boldsymbol{\omega}_e^T \boldsymbol{\omega}_e \\ &\quad - c k_\Theta \mathbf{n}_e^T \mathbf{p}_{e,2} - c k_\omega \mathbf{n}_e^T \boldsymbol{\omega}_e. \end{aligned} \quad (33)$$

This expression can be upper bounded as

$$\begin{aligned} \dot{V}_2 &\leq -k_\Theta^{-1} k_\omega \|\boldsymbol{\omega}_e\|_2^2 + c \|\boldsymbol{\omega}_e\|_2 \|\mathbf{n}_e\|_2 + \frac{1}{2} c \|\boldsymbol{\omega}_e\|_2^2 \\ &\quad - c k_\Theta \|\mathbf{n}_e\|_2^2 + c k_\omega \|\mathbf{n}_e\|_2 \|\boldsymbol{\omega}_e\|_2, \end{aligned} \quad (34)$$

because $-\|\mathbf{n}_e\|_2^2 \geq -\|\mathbf{n}_e\|_2 \|\mathbf{p}_{e,2}\|_2$, for any $\Theta_e \in [0, 2\pi)$ —the operational range selected by design. Last, using matrix manipulation rules, we obtain

$$\dot{V}_2 \leq -\mathbf{x}_e^T \begin{bmatrix} c k_\Theta & -\frac{1}{2} c (k_\omega + 1) \\ -\frac{1}{2} c (k_\omega + 1) & k_\Theta^{-1} k_\omega - \frac{1}{2} c \end{bmatrix} \mathbf{x}_e, \quad (35)$$

where $\mathbf{x}_e = [\|\mathbf{n}_e\|_2 \ \|\boldsymbol{\omega}_e\|_2]^T$.